EXAMINING RAPID DEPRESSURIZATION OF HONEYCOMB PANELS USING COMPUTATIONAL FLUID DYNAMICS THROUGH ANISOTROPIC POROUS MODELING

Max Hewkin-Greggor[1], Parthiv Shah, Scott Kidney
ATA Engineering, Inc., San Diego, CA, 92128

Adam Dybek, Sam LeeDuMez
Sierra Space Corporation, Louisville, CO, 80027

ABSTRACT

A computational fluid dynamics (CFD) methodology has been developed for modeling the rapid depressurization of composite honeycomb panels, using single-cell resolved simulation and whole-panel porous modeling, Figure 1. The workflow has been validated against flow network modeling and experimental data.

Composite honeycomb panels are often used in the solar arrays of satellites and spacecraft. During launch sequences, these panels experience rapid atmospheric depressurization, resulting in an elevated pressure differential between honeycomb cells and atmosphere that could compromise panel integrity. The industry standard method to reduce differential pressure is to perforate the honeycomb cell walls to allow venting between cells. The predominant existing method for sizing perforations is a simplistic design rule for venting that is not suitable for honeycomb panels during modern launch cycles [1]. A review of literature suggests that there has been only limited use of advanced computer-aided engineering tools for honeycomb panel venting. Thus, the goal of this project was to develop a method for predicting differential pressures using CFD.

The flow through a honeycomb panel during a depressurization event is complex and transient by nature; fully resolved CFD of an entire panel is therefore not feasible. The problem was instead simplified in several stages. First, a unit-cell steady CFD model made in Siemens Simcenter STAR-CCM+ characterized flow through a single perforated honeycomb wall of an industrially representative panel. This characterization was used to calculate equivalent porous resistance coefficients. Separately, the same resistance coefficients were calculated using 1D theory and corroborated the CFD values within 12.5%. The resistance coefficients from the unit-cell CFD model were input to a second CFD model of the whole panel as a simplified orthotropic porous medium. This time-accurate model was run for the depressurization event, and the maximum pressure differential was logged. The methodology was designed for fast turnaround. It could be applied to a new panel geometry and return results within one working day.

Additionally, Siemens Simcenter Amesim was used to develop a 1D flow network model of the same panel. The maximum pressure differential was within 12% of the CFD model result. The CFD methodology was also validated against available data from experimental tests in which a sealed honeycomb panel was evacuated from a single location. The results showed agreement within the experimental uncertainty, thereby demonstrating how this workflow provides a powerful, rapid new tool in the design of honeycomb panels.
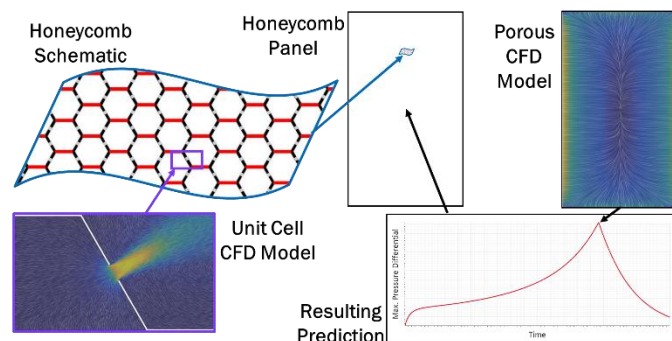
Figure 1. Workflow for depressurization modeling

---

[1] Corresponding author; mhg@ata-e.com

NOMENCLATURE

1D	one dimensional
2D	two dimensional
3D	three dimensional
A_o	orifice area
A_s	superficial flow area
CAD	computer aided design
C_D	orifice discharge coefficient
CFD	computational fluid dynamics
CPU	central processing unit
$[\ ]_d$	downstream
d_c	honeycomb cell size
D_o	orifice (perforation) diameter
h	honeycomb through thickness (does not include face sheet)
l	honeycomb cell wall length
L_ξ	core-ribbon direction orifice spacing
$L_\_$	distance travelled in _ direction
L_η	ribbon-orthogonal direction orifice spacing
$\dot{m}$	mass flow rate
muf	model uncertainty factor
N_o	number of orifices per wall
p	pressure
P_i	porous inertial resistance coefficient
P_v	porous viscous resistance coefficient
RANS	Reynolds-averaged Navier-Stokes
$[\ ]_{ref}$	reference condition
STAR	Siemens Simcenter STAR-CCM+
t	honeycomb film gauge
$[\ ]_u$	upstream
u_o	orifice velocity
u_s	superficial velocity
$\dot{V}$	volumetric flow rate
y+	dimensionless wall distance
Z	spanwise/thickness direction
$[\ ]_\eta, [\ ]_y$	ribbon-orthogonal direction
$[\ ]_\xi, [\ ]_x$	core-ribbon direction
ρ	density

INTRODUCTION

Composite honeycomb panels are used in solar arrays that experience rapid atmospheric depressurization during launch sequences. Elevated pressure differential between honeycomb cells and atmosphere can compromise panel integrity by causing inter-cell wall failure or a honeycomb–to–face-sheet bond failure, potentially leading to structural failure. Cell vent holes are a passive method used in honeycomb panels to ensure that pressure is equalized across cells interior to the substrate and ultimately, through the exposed core at the panel edges, to the ambient environment, Figure 2. If venting is still insufficient, face-sheet vent holes are a more drastic method of pressure differential mitigation but are preferably avoided.
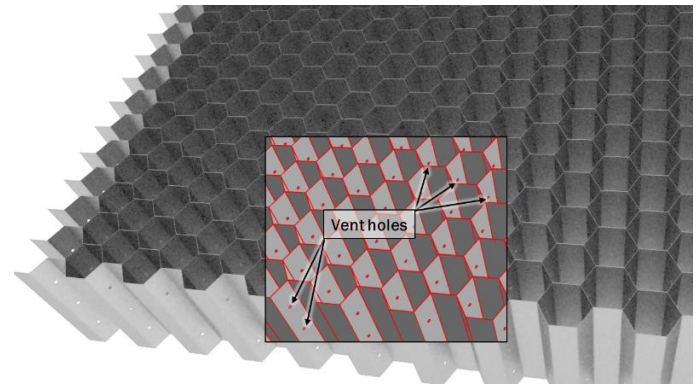
Figure 2. CAD model of aluminum honeycomb minus face sheets, illustrating cell wall venting.

A 1993 report by Epstein and Ruth [2] documents known anomalies with unvented honeycomb sandwich structures on spacecraft such as Mariner 3, Titan III, the Block II Global Positioning System satellite, and the Atlas-Centaur payload fairings. The report recommends that optimal venting is such that there is "practically no pressure differential."

Achieving proper venting for a spacecraft structure may be as simple as proper sizing of vent holes, but proper venting can become more complex if the venting follows a tortuous path such as in a honeycomb panel, or as space hardware requirements dictate, for example, if other factors such as transmission of particles must be considered. The experimental work of Mironer and Regan [3] for the evacuation of a one-cubic-foot tank via a single orifice plate resulted in a design plot that was used for venting of Space Shuttle launch payloads. This study also led to the use of a rule of thumb, which has potentially been misinterpreted by others as being more widely applicable than to just single-tank, single-orifice evacuation [1].

Sufficient venting of panels is critical, and validation of the panel venting design by test is expensive and not practical to support manufacturing schedules, requiring design validation by analysis. Unlike a simple venting arrangement, a honeycomb panel results in a complex flow network of many vent holes both in series and in parallel and requires more advanced analysis methods. A review of literature on spacecraft hardware venting analysis

suggests limited use of advanced computer-aided engineering tools in honeycomb panel venting. A 2021 paper by Schweickart and Devaud [1] is a notable exception; they used the SINDA/FLUINT flow network modeling software to simulate launch depressurization by modeling individual cell volumes connected by small orifices. The analysis was supported by honeycomb depressurization testing. Separately, the effect of honeycomb sandwich panel differential pressure on panel failure has been analyzed by Rinker et al. [4]. That analysis method would be the logical application of pressures obtained from a fluid venting analysis if the panel was expected to be close to failure.

To the authors' knowledge, three-dimensional (3D) simulation methods such as computational fluid dynamics (CFD) have not been used to date to simulate honeycomb panel venting, perhaps due to the perceived complexity in explicit geometric representation of an array of hundreds, or thousands of individual cells. Many modern CFD codes such as Siemens Simcenter STAR-CCM+ (STAR) allow the modeling of complex arrays of cellular structures as equivalent porous media. The porous resistance values may be defined in detailed, 3D breakout simulations and then treated at a more macroscopic level as a medium with directionally dependent fluid flow constitutive properties. Thus, the goal of this paper was to develop a method to predict differential pressures using CFD, with verification to a flow network model and to experimental data to bolster confidence in the methods.

ANALYSIS APPROACH

Fully resolved CFD of the complex, transient flow in an entire panel for tens of seconds is not feasible within a typical design process timeframe. The problem was therefore simplified by splitting the analysis into two stages. First, a unit cell CFD model was used to characterize mass flow versus pressure drop through a single perforated honeycomb wall at several different driving pressures. The results of

this unit cell model were used to calculate equivalent porous medium resistance coefficients for the whole honeycomb panel. Separately, one-dimensional (1D) theory was used to calculate the same resistance coefficients and corroborate the values calculated from the CFD model. The resistance coefficients from the unit cell model were then used as an input to a second CFD model of the honeycomb panel as a porous medium. This time-accurate model was able to run for the whole depressurization event, due to the simplification of the complex geometry as a porous medium.

A second analysis method, to act as a validation for the CFD, used a 1D flow network model of the panel developed in Siemens Simcenter Amesim. The behavior of groups of individual cells was first characterized by modeling each hexagonal cell of the honeycomb using a simple pneumatic chamber with heat exchange and four ports for wall venting. This characterization allowed groups of cells to be represented by a single pneumatic chamber, many of which could then be linked to represent a quarter panel on which the full depressurization could be run.

Geometry

For the methodology development, an industrially representative honeycomb panel was used. Composite honeycomb panels are made up of a honeycomb center fixed to a sheet on either open face. The face-sheet dimensions of the panel used were 1.8 m × 1.07 m. The honeycomb is assumed to be constructed from Aluminum 5056 film, of 17.8 um gauge, that is shaped and glued to form honeycomb, that is 12.7 mm thick with a 3.175 mm cell size. Cell size, d_c, is the parallel distance between the two joined walls in the cell, Figure 3. Honeycomb thickness is the into-page dimension. Each non-joined wall of the honeycomb is assumed to be perforated by three equally spaced holes of 0.254 mm in diameter, as is industry standard. These holes are assumed to be a sharp-edged orifice. The hole diameter is a critical dimension, because total vent area per wall is the principal limiter for venting rate.
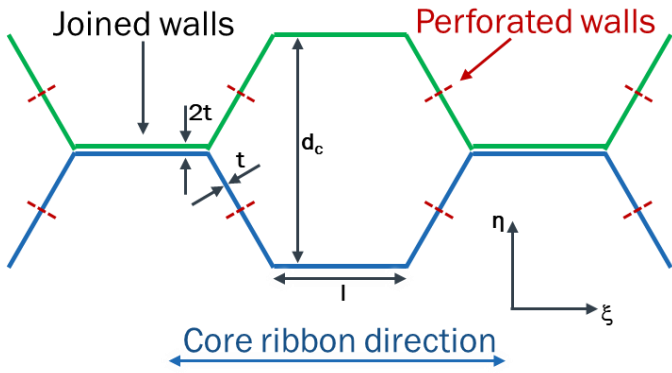
Figure 3. Honeycomb geometry perforation layout and nomenclature.

Figure 4. Distance traveled in principal directions (left, purple solid arrows) and actual tortuous routes (left, blue dotted arrows). Simple sudden expansion model of perforation (right). Dashed control volume represents a unit cell that can be mirrored and periodically repeated.

Table 1. Key dimensions and parameters.

Dimension	Description	Value
h	honeycomb through thickness (does not include face sheet)	0.0127 m
D_o	orifice (perforation) diameter	2.54e-4 m
$A_o = \pi D_o^2$	orifice area	5.06707e-8 m^2
C_D	orifice discharge coefficient (assuming sharp edged orifice at Re of interest, corroborated by breakout CFD results)	0.67
N_o	number of orifices per wall	3
L_ξ	core-ribbon direction orifice spacing	2.7291e-3 m
L_η	ribbon-orthogonal direction orifice spacing	1.5875e-3 m

Depressurization Conditions

The panel is assumed to be equilibrated with standard atmospheric conditions (101.3 kPa, 295.3 K) at time = 0 s. Beginning at time = 0 s, the atmospheric pressure drops at a rate of 6900 Pa/s; therefore, at time = 14.7 s, pressure levels are negligible. Atmospheric pressure then remains negligible as the panel continues to vent. Atmospheric temperature is assumed to remain constant throughout for simplicity.

ANALYTICAL HONEYCOMB MODEL

Modeling the honeycomb's network of orifices as an equivalent porous medium requires determination of the equivalent porous resistance coefficients through the honeycomb. In addition to using a breakout CFD model to do this, these values were derived using basic flow theory for a sanity check. The basic flow is described by flow through an orifice followed by sudden expansion. The air encounters pressure losses as the orifice holes are crossed. Viewed as a porous medium, the flow has resistance in two primary directions: the core-ribbon direction, ξ, and the ribbon-orthogonal direction, η, Figure 4 (left). The fluid encounters one orifice every L_ξ in the ξ-direction, and every L_η in the η-direction. To derive the orthotropic porous resistance for each direction using theoretical arguments requires the key panel dimensions given in Table 1.

Calculating the Orifice Velocity

Porous medium resistance is based on a bulk velocity through the medium instead of local velocity through each orifice. Assuming a low-speed, isothermal flow, consider the basic flow problem in a unit cell, Figure 4 (right). A pressure difference Δp exists between upstream and

downstream pressures p_u and p_d. It is assumed that the flow is locally incompressible, i.e., the density of a fluid particle changes very slowly relative to the timescale over which fluid passes from one cell to the next. Globally across the panel, the pressure will change appreciably in space and time, so a thermodynamic equation of state may be written as $p = (const) \times \rho$. The mixed-out velocity in each hexagonal cell is approximately zero. Per Bernoulli's equation, the flow expands to pressure p_d and orifice velocity u_o, at an orifice vena contracta of area $C_D A_o$, for each of N_o orifices:

$$p_u = p_d + \frac{\rho u_o^2}{2} \implies u_o = \sqrt{\frac{2\Delta p}{\rho}} \qquad \textbf{Equation 1}$$

Calculating the Inertial Porous Resistances (Pi)

For this sanity check, the viscous contribution to resistance is assumed to be small. Using volume conservation (for this low Mach number flow), the bulk (superficial) velocity u_s can be calculated based on the unit cell panel cross-section area A_s in each direction by assuming that the honeycomb porosity is approximately 1 (i.e., the foil does not occupy a significant proportion of volume):

$$\dot{V} = u_o(C_D N_o A_o) = u_s A_s \qquad \textbf{Equation 2}$$

$$u_{s\xi} = u_o\left(C_D N_o \frac{A_o}{A_{s,\xi}}\right) = u_o\left(C_D N_o \frac{A_o}{L_\eta h}\right) \qquad \textbf{Equation 3}$$

$$u_{s\eta} = u_o\left(C_D N_o \frac{A_o}{A_{s,\eta}}\right) = u_o\left(C_D N_o \frac{A_o}{L_\xi h}\right) \qquad \textbf{Equation 4}$$

To calculate the porous resistance coefficients, it is necessary to formulate the pressure drop per unit length in each principal direction based on the bulk velocity in the porous medium. This formulation can be done by first substituting for Δp using Equation 1 and then for u_o using Equation 2 thorough Equation 4. The geometric constants form the porous inertial resistance coefficients.

$$\frac{\Delta p}{L_\xi} = \frac{\rho u_o^2}{2L_\xi} = \left(\frac{\rho}{2L_\xi}\right)\left[\frac{L_\eta h}{C_D N_o A_o}\right]^2 u_{s\xi}^2 = P_{i\xi} u_{s\xi}^2 \qquad \textbf{Equation 5}$$

$$\frac{\Delta p}{L_\eta} = \frac{\rho u_o^2}{2L_\eta} = \left(\frac{\rho}{2L_\eta}\right)\left[\frac{L_\xi h}{C_D N_o A_o}\right]^2 u_{s\eta}^2 = P_{i\eta} u_{s\eta}^2 \qquad \textbf{Equation 6}$$

Given the geometric parameters in this case, Table 1, and atmospheric conditions of 101.3 kPa atmospheric pressure, 295.3 K temperature and 1.195 kg/m³ density, the resistance coefficients are calculated as:

$$P_{i\xi} = \left(\frac{\rho}{2L_\xi}\right)\left[\frac{L_\eta h}{C_D N_o A_o}\right]^2 = 8.58 \times 10^6 \ \frac{kg}{m^4} \qquad \textbf{Equation 7}$$

$$P_{i\eta} = \left(\frac{\rho}{2L_\eta}\right)\left[\frac{L_\xi h}{C_D N_o A_o}\right]^2 = 4.36 \times 10^7 \ \frac{kg}{m^4} \qquad \textbf{Equation 8}$$

BREAKOUT CFD MODEL TO DETERMINE POROUS RESISTANCE COEFFICIENTS

To improve the accuracy of the porous resistance coefficients estimated using basic theory, a breakout CFD model of a single perforated wall was used to characterize the flow. This characterization gave the relationship between mass flow rate and driving pressure. This relationship was then fit to a polynomial curve to quantify the effective porous resistance coefficients. All CFD was run using STAR version 2210.

Simulation Configuration

The simplest, tessellating, and symmetrical substructure of the honeycomb is composed of two quarter cells with a single perforated wall in the middle. The mass flow rate at a range of driving pressures is required; this can be determined from a series of steady simulations. The CAD geometry of several hexagonal cells and the extracted fluid volume of the breakout domain are shown in Figure 5 (left and center respectively). The extracted breakout domain was discretized into a computational mesh using the automated polyhedral mesher in STAR. The near-wall flow was resolved (with y+<1). The resulting mesh has a cell count of approximately 490,000, Figure 5 (right). This resulted in a typical steady run time of approximately 45 minutes on 16 central processing units (CPUs).

The breakout model was configured to solve three-dimensional, steady-state Reynolds-averaged

Navier-Stokes (RANS) models. The air was treated as an ideal, compressible gas, with default atmospheric air material properties. Flow was assumed to be fully turbulent, modeled using the k-omega SST turbulence model. The all y+ wall treatment model was used, although as previously stated, the mesh was wall-resolved. All walls were assumed to be adiabatic. Boundaries on the upstream side of the perforated wall were defined by stagnation conditions of 101.3 kPa pressure and 295.3 K temperature, Figure 6. Boundaries on the downstream side of the perforated wall were described by static conditions using prescribed pressure drop and a temperature of 295.3 K.
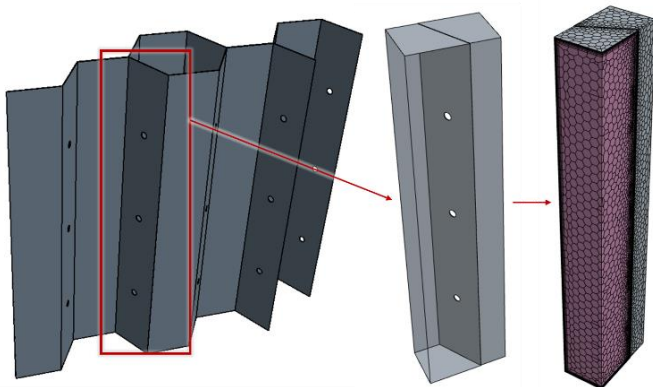
Figure 5. CAD model of honeycomb showing aluminum foil (left), quarter-hex breakout model showing fluid volume (center) and polyhedral CFD mesh (right).
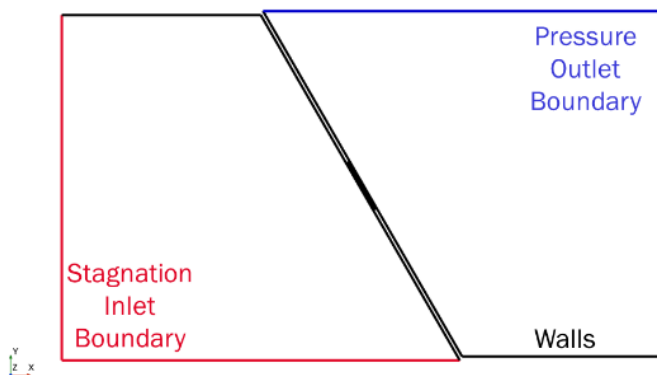
Figure 6. Schematic of boundary conditions.

Results

The steady simulation was run seven times for different driving pressures ranging from 0.1 Pa to 10,000 Pa. The range of driving pressures resulted in orifice Reynolds numbers varying from 1.3 to 1550, later found to cover the range of equivalent values seen in the porous model. Contours of velocity, superposed with line integral convolutions of velocity vectors, are shown for the extreme cases in Figure 7. A monotonic change in the vena contracta was seen as the driving pressure difference increases. The mass flow resulting from the prescribed driving pressure was extracted from each simulation result.
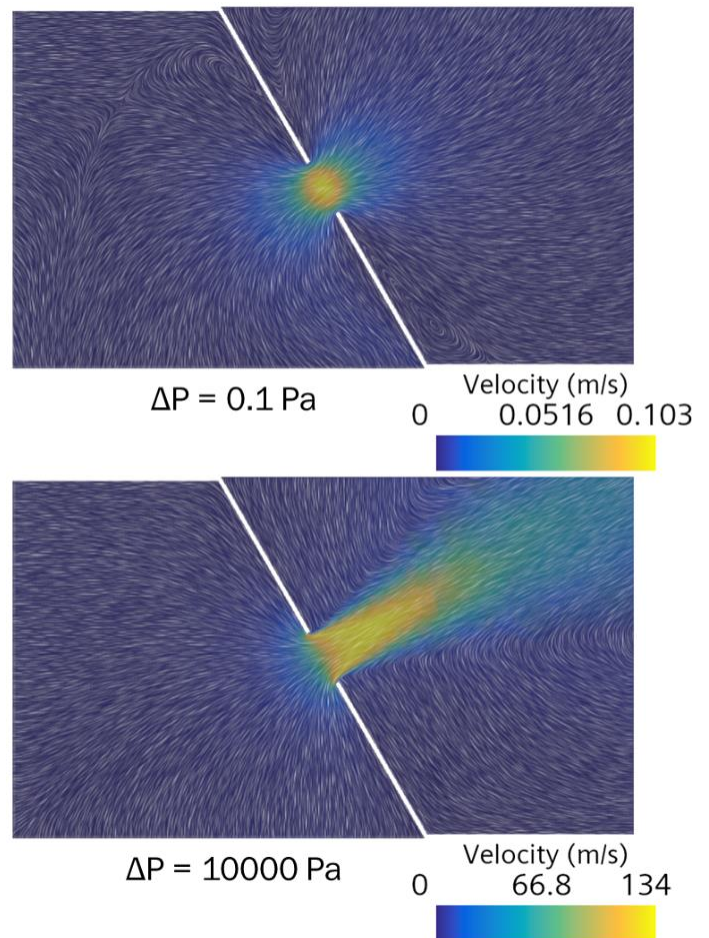
Figure 7. Velocity contours and line integral convolutions on cut plane through center of central perforation of breakout model, for two pressure differentials. Note different color scales.

Porous resistance coefficient calculation

The pressure drop due to the flow passing through the perforated walls is assumed to be described by

$$\Delta p = P_i u^2 + P_v u \qquad \textbf{Equation 9}$$

The modification of Equation 9 to fit a continuous pressure drop over a given length traveled, Δp/ΔL, with a superficial flow velocity, u_s, in the two principal directions gives

$$\frac{\Delta p}{\Delta \xi} = P_{i\xi} u_{s\xi}^2 + P_{v\xi} u_{s\xi} \qquad \textbf{Equation 10}$$

$$\frac{\Delta p}{\Delta \eta} = P_{i\eta} u_{s\eta}^2 + P_{v\eta} u_{s\eta} \qquad \textbf{Equation 11}$$

where $\Delta \xi$ and $\Delta \eta$ are the lengths of the breakout domain in the X and Y direction, respectively, and:

$$u_s = \frac{\dot{m}}{\rho A_s} \qquad \textbf{Equation 12}$$

Polynomials of the forms of Equations 10-11 were fitted to the results of the breakout CFD model, Figure 8. A second set of polynomials with the viscous resistance coefficient set to 0 was also fitted, and demonstrated minimal difference, suggesting that for this case the viscous term can be neglected at the flow rates and Reynolds numbers of interest. This resulted in the following inertial coefficients for the transient porous simulation:

$$P_{i\xi} = \left(\frac{\rho}{\rho_{ref}}\right) 9.662 \times 10^6 \ \frac{kg}{m^4} \qquad \textbf{Equation 13}$$

$$P_{i\eta} = \left(\frac{\rho}{\rho_{ref}}\right) 4.956 \times 10^7 \ \frac{kg}{m^4} \qquad \textbf{Equation 14}$$

where ρ_{ref} is density of breakout simulations and ρ is the density at any given time in the transient porous simulations. This density correction is necessary for the transient simulation, because while the density does not vary much spatially, it will vary considerably over the time of the simulation. These values are both within 12.5% of those derived from 1D theory, providing confidence in the validity of both models. This agreement is particularly close when considering that the discharge coefficient for a sharp orifice in the literature varies from 0.61 to 0.67. The chosen value in the analytical model need only be adjusted from 0.67 to 0.63 and the result would match the CFD within 1%.
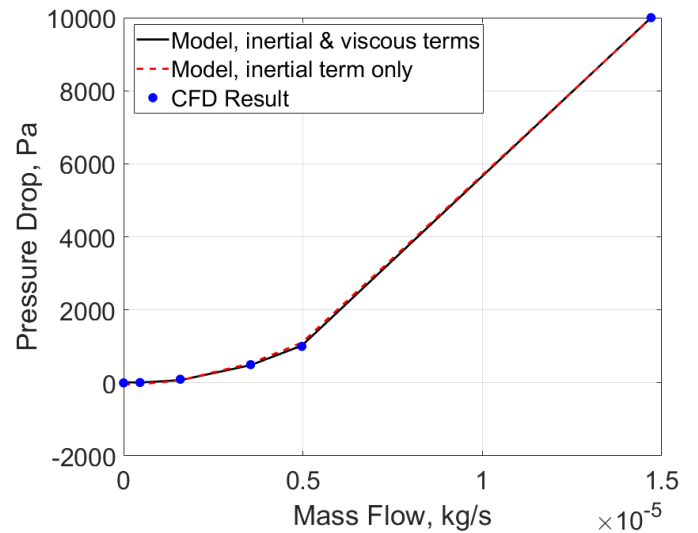
Figure 8. Pressure drop vs. mass flow from CFD breakout model result and the fitted polynomials using resistance coefficients.

Verifications and Sanity Checks

To confirm that the derived density scaling is appropriate, a further breakout case was run, with 10% of the original inlet density and comparative 1000% delta pressure, so that Δp/ρ remains fixed. Comparing the two cases, the mass flows are consistent within 0.26%; this confirms that derived porous resistances will scale with local density as expected.

To confirm that the boundary condition/flow direction setup did not affect the predicted mass flow significantly, the breakout simulations were re-run with symmetry planes along first the constant X boundaries and then the constant Y boundaries. The resulting mass flow for a given driving pressure did not change by more than 0.06%. This indicates that the result is insensitive to whether flow is predominantly moving in the core-ribbon direction or the ribbon-orthogonal direction.

Finally, to substantiate that the breakout model was producing reasonable discharge coefficient values as a function of orifice diameter Reynolds number (Re_{D_o}), the CFD results were compared to an empirical model (Equation 15) for C_D given in Wu et al. [5], Figure 9. It was concluded that the CFD

captured the relationship well in terms of qualitative trend, as well as peak discharge coefficient value (0.67 versus 0.69).

$$C_d = 0.61 \left(1 + 1.07e^{-0.126\sqrt{Re_{D_o}}} - 2.07e^{-0.246\sqrt{Re_{D_o}}}\right)$$ **Equation 15**
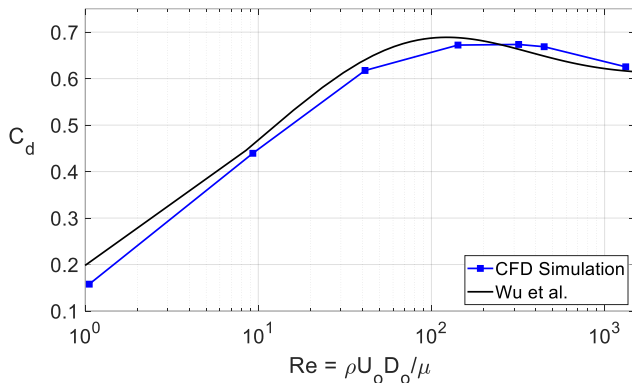
Figure 9. Comparison between computed discharge coefficient and empirically derived correlation based upon Fig. 3 of Wu et al. [5]

FLOW NETWORK MODEL

A 1D flow network model of the panel was developed in Siemens Simcenter Amesim. Each hexagonal cell of the aluminum honeycomb core was modeled using a simple pneumatic chamber with heat exchange and four ports, Figure 10 (top). Wall venting on four of the six cell walls was modeled with pneumatic orifices with a constant flow coefficient. The volume of the hexagon cell was calculated to be 1.11e-7 m³ and the orifice area of each orifice was 5.1e-8 m², representing three vent holes on each of the four vented walls. The flow discharge coefficient was set to 0.67, as calculated from the breakout CFD model results.

It is computationally infeasible to model every hexagonal cell, even in a quarter panel model. To reduce the computational burden, a breakout approach was used once again. A grid of 55 hexagonal cells was modeled using 55 pneumatic chambers and orifices. These 55 chambers were then themselves represented by one equivalent simple pneumatic chamber with heat exchange and four ports and four orifices, Figure 10 (top). The orifice area of each of the four orifices in the

equivalent chamber was multiplied by a model uncertainty factor (muf), to represent the additional flow restrictions experienced by the group of 55 hexagonal cells. The muf was tuned through an automated trade-study routine to match the top left corner pressure of the group of 55 chambers with the pressure in the single equivalent chamber. The tuning occurred at peak external to internal differential pressure at time equal to 14.67 s and resulted in an uncertainty factor of 0.57. Groups of a single equivalent chambers and orifices were then linked to represent a quarter panel, Figure 10 (bottom), with either plugged-edge conditions, for internal panel symmetry, or vented-edge conditions, for exposed edges. The pressure in the chamber at the top left of the quarter-panel model represents the peak pressure in the panel. This pressure was logged and is compared to the transient CFD result in the following section.
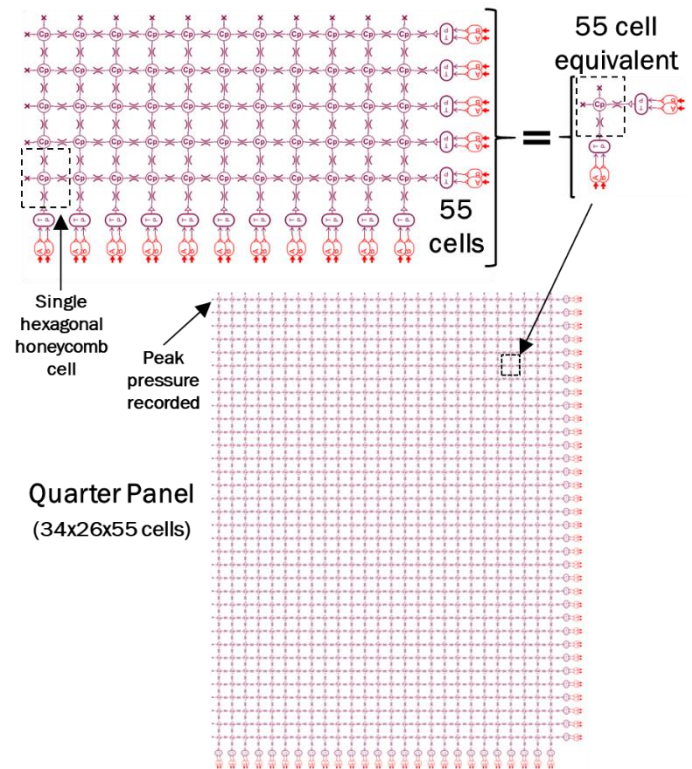
Figure 10. Fifty-five cells (top left) are represented by an equivalent model with one pneumatic chamber (top right). Combining equivalent chambers allows creation of a quarter panel model (bottom).

TRANSIENT POROUS CFD MODEL

Through use of the porous modeling capability of STAR, the honeycomb panel (excluding face sheets) can be represented using a simple cuboid, Figure 11. The complex internal geometry is accounted for by applying the porous inertial resistance coefficients derived from the breakout model results.

Simulation Configuration

The geometry was meshed using the trimmed cell mesher to ensure a regular mesh of minimal cell count, Figure 11. The mesh is only one cell thick in the thickness direction because the porous model accounts for all viscous resistances, such that modeling viscous effects, including boundary layers, is not necessary. This results in a cell count of approximately 21,000. The fluid is initialized to 101.3 kPa and 295.3 K with zero velocity. Atmospheric pressure is prescribed on the four outer boundaries and controlled according to the prescribed profile of a linear drop from 101.3 kPa to 483 Pa over 14.63 s. The simulation cannot go to exactly zero pressure due to limitations of the solver. Atmospheric temperature is held constant.

The physics used for the transient model are necessarily different from those of the breakout model. The flow is modeled as three-dimensional but is technically quasi–two-dimensional (2D) due to the mesh used. Air is modeled as an ideal gas with standard material properties, but assumed to be inviscid. This inviscid assumption is necessary because, once again, all the viscous resistances are accounted for by the porous inertial resistances that are input into the porous media model. The air and honeycomb material are assumed to be in thermal equilibrium. The face-sheet walls were treated as adiabatic. Porosity is set according to the film/air volume ratio of 0.9851. Porous resistance coefficients are set according to the breakout model. The tortuosity is set to unity, as any effects of tortuosity are captured in the resistance coefficients. The simulation runs time-accurate,

with 2 ms timesteps, for 20 s of flow. This takes approximately 8.2 hours to run on 8 CPUs.

To confirm that the porous media model was correctly configured, the setup was applied to the breakout model with the internal walls removed. The resulting mass flows for each driving pressure varied by no more than 6.5% from the original values. This indicates that the porous model approach will predict the flow in the overall panel model with a similar accuracy to one that resolved every honeycomb wall and perforation.

To validate many of the other CFD configuration choices made, a second model was run using a different mesh strategy (coarser in XY, but several spanwise cells), a different porous media setup (STAR porous region instead of porous media), isothermal conditions, a longer timestep, and less stringent convergence criteria. The maximum overpressure predicted by this model agreed with the original model within 4.5%, giving confidence that the result is not sensitive to the exact chosen configuration.
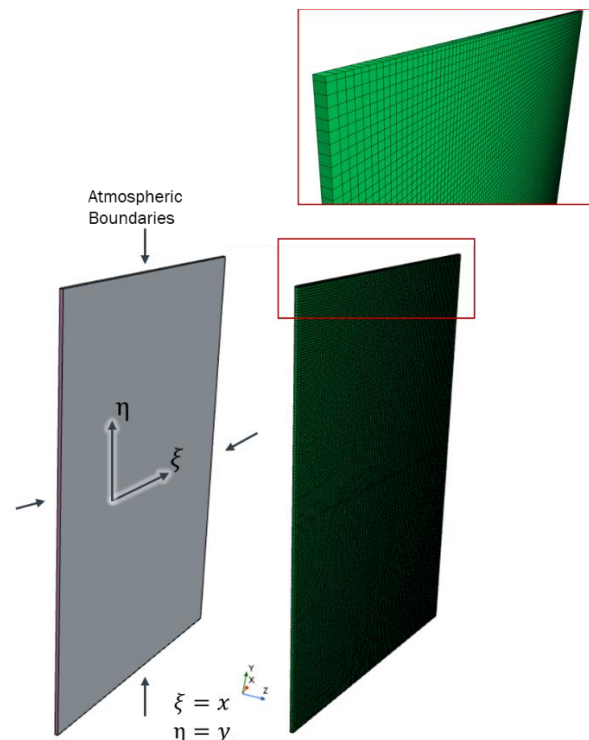
Figure 11. Domain geometry and mesh detail for transient porous CFD model.

Results

A series of snapshots in time of the pressure differential between atmosphere and the air inside of the panel, and the velocity field are shown in Figure 12. Note that the pressure contours are shown on a log scale to better discern the large variation within the panel. The time points show the flow field at 50% atmospheric pressure, at the end of atmospheric pressure drop, and at the end of the simulation. The effect of the core-ribbon direction is clear in the velocity line integral convolutions, which show that, due to the reduced resistance in the X direction, the flow predominantly moves in the X direction, except when close to the short edge boundaries. The resulting maximum pressure differential in the panel versus time was compared to the flow network result, Figure 13. The highest maximum over-pressure is predicted by the CFD model as 11.2 kPa at time = 14.7 s. This occurs at the center of the panel. The CFD result is within 12% of the predicted value of 9.86 kPa from the flow network model.
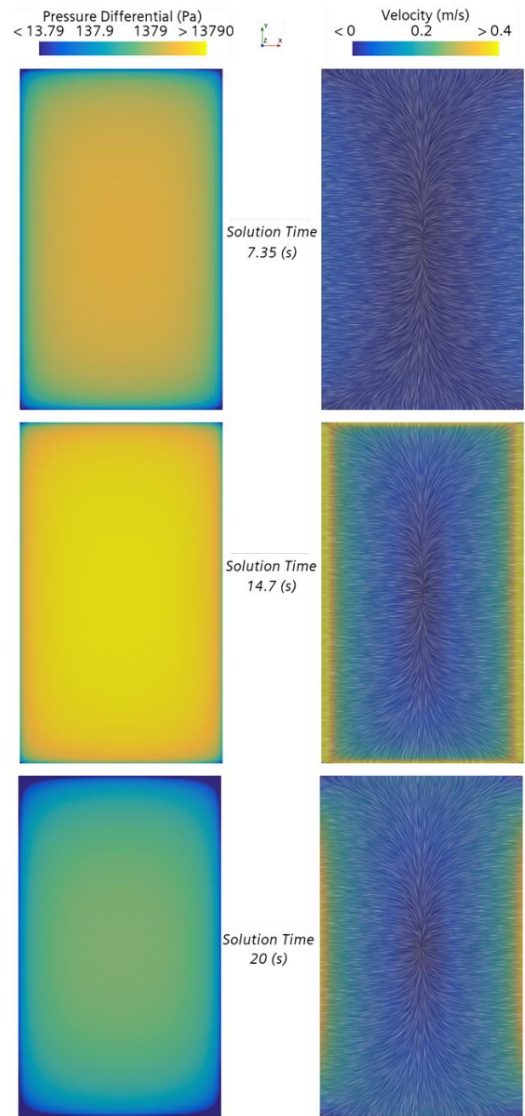
Figure 12. Local pressure differential and velocity at several time points during transient simulation.
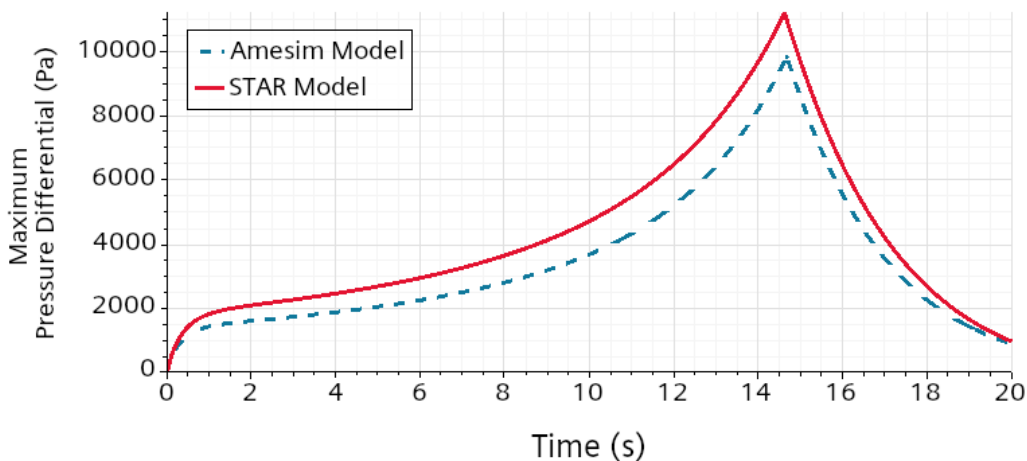
Figure 13. Maximum local pressure differential vs. time for flow network (Amesim) and CFD (STAR) models.

EXPERIMENTAL VALIDATION

To provide further validation for the CFD methodology, it was applied to the geometry used by Schweickart and Devaud [1] in their experimental tests. These tests measured the pressure at several ports along a 1.22 m × 0.10 m sealed honeycomb panel, with internal thickness of 22.3 mm, as it was evacuated from a single vacuum point, Figure 14. The honeycomb has a cell size of 6.35 mm, with four perforations of 0.13 mm per wall. Schweickart and Devaud themselves used a flow network approach to model the test, getting reasonable agreement after tuning the hole size until the best match was achieved. Their justification for adjusting hole size in their model was that there is manufacturing uncertainty of 0.13–0.15 mm. Additional uncertainty is added to this modeling study, because Schweickart and Devaud do not state the film gauge or vacuum zone radius in their paper. These two parameters were instead estimated from photos and figures in their paper as 63.5 um and 5.7 mm respectively, although there is likely error on the order of 10–20% in these values. Finally, uncertainty in results comparison is further increased due to the use of manual instrumentation. Therefore, the experimental error margins may be higher than usual, but nevertheless the results still provide a useful benchmark against which to compare the CFD.

The CFD approach for both the breakout and porous models was identical to the previously outlined methods, except that the porous model timestep was increased from 2 ms to 5 ms, to accommodate the 10× longer flow run time. The first few seconds were run at both timesteps and demonstrated that the increased timestep had no detrimental impact on convergence. Other than geometric and boundary condition changes, the only other difference was the replacement of external boundaries on the porous model with walls and a single evacuation point.

Figure 14. Sealed panel geometry, indicating vacuum point and pressure measurement ports.

Fitting porous resistance coefficients to the results of the breakout model simulations required inclusion of a non-zero viscous coefficient to achieve an acceptable fit, Figure 15. The driving reason for this is the 74% reduction in perforation area compared to the previous panel. The resulting coefficients are $P_{i\eta}$ = 1.65e9 kg/m^4, $P_{i\xi}$ = 3.05e8 kg/m^4, $P_{v\eta}$ = 3.13e6 kg/m^3-s, and $P_{v\xi}$ = 1.02e6 kg/m^3-s. These inertial values represent a factor of 32 increase compared to the previous panel. Given that the cell size is doubled, and yet this increase is still seen, demonstrates that hole size is a critical dimension in determining vent rate. Running the porous model for this geometry, with these calculated coefficients, presented a good match with the experimental data, displaying a maximum error of +4% at port 7 at 24.8 s, Figure 16.
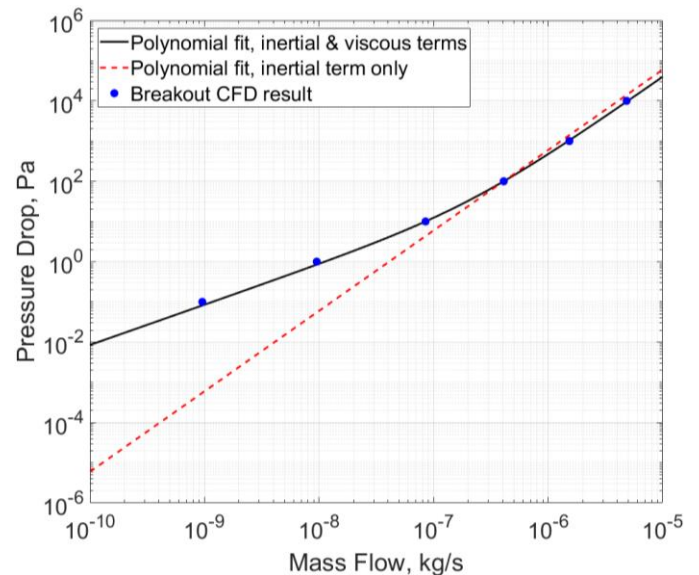
Figure 15. Breakout model pressure drop vs. mass flow and fitted polynomials. Including the viscous term is important at this smaller perforation size.
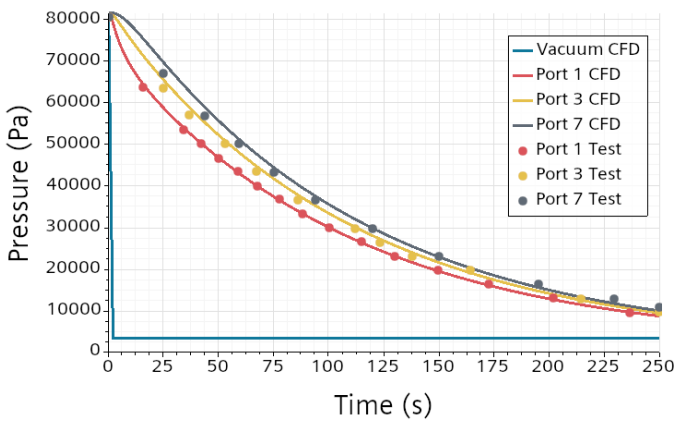
Figure 16. CFD vs test data for the sealed panel depressurization.

To determine the sensitivity of the results to the uncertain geometric factors (film gauge, hole size, and vacuum area), the simulations were repeated three times. First, the hole diameter was increased from 0.13 mm to 0.14 mm (the value selected by Schweickart and Devaud to best match one of their models to the test data); this resulted in a 32% reduction in inertial resistance coefficients and a 30% reduction in viscous resistance coefficients. Second, and with this larger hole diameter, the vacuum area was doubled; resistance coefficients were further unaffected by this as the honeycomb structure is not changed. Third, with the original hole diameter, the film gauge was reduced by a factor of 25 to 2.54 um; this resulted in an 8%

increase in inertial coefficients and a 60% reduction in viscous coefficients. The impact of these three changes on the depressurization prediction at ports 1 and 7 is shown in Figure 17. Changing the film gauge had limited effect on the result, indicating that while the viscous resistance coefficient may be important at low flow rates, for this depressurization schedule, the flow remains inertially dominated and therefore not sensitive to film gauge. Increasing the hole size caused significant increase in venting and therefore departure from the test data. Further disparity was caused by then doubling the vacuum area. This result further confirms the sensitivity of vent rate to hole size, and in this test scenario, vacuum area. It should be noted that it is possible that the real geometry has a smaller vacuum area and a larger hole size and this would balance out to again match the test data. Nevertheless, given the manual instrumentation used for the test, the baseline results likely lie within the experimental uncertainty. The results of this study therefore provide further validation that the CFD methodology developed here correctly captures the complex flow within honeycomb panels undergoing rapid depressurization.
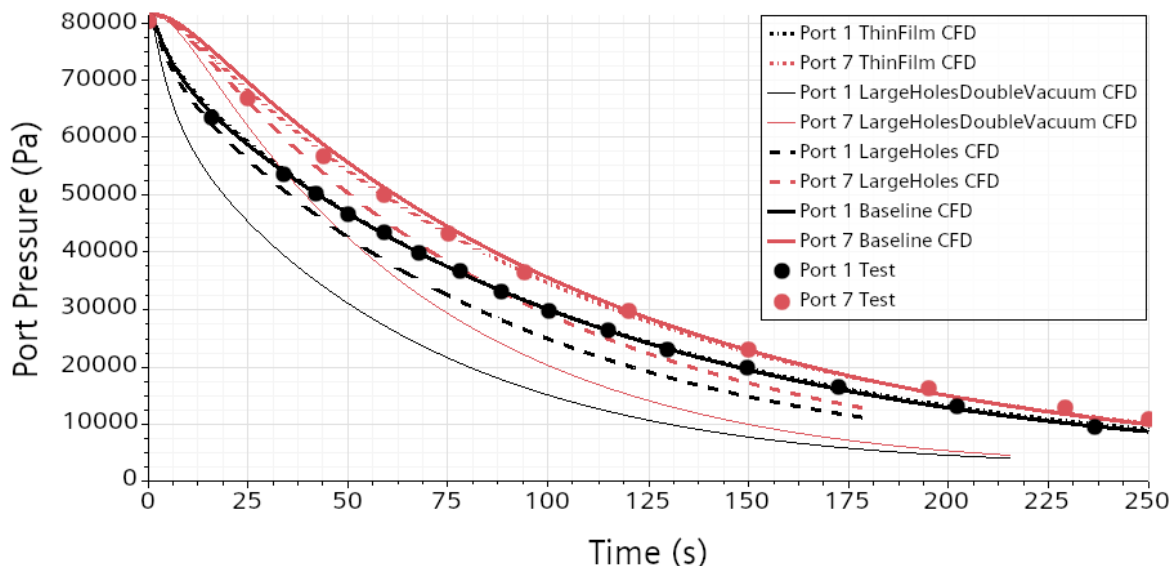
Figure 17. Depressurization comparison between test data and four CFD cases with varying geometric parameters. The thin film model provides the closest match.

CONCLUSIONS

Composite honeycomb panels are often used in solar arrays that experiences rapid atmospheric depressurization during launch sequence. Perforations are added to honeycomb cell walls to allow venting between cells. Previous work published in the open literature does not include the use of CFD for honeycomb panel venting predictions. This paper described a CFD methodology for modeling the rapid depressurization of composite honeycomb panels.

The flow through the honeycomb panel during the depressurization event is complex and transient by nature. Fully resolved CFD of the entire panel is therefore not feasible, so the problem was simplified. A unit cell Siemens Simcenter STAR-CCM+ CFD model was used to characterize flow through a single perforated honeycomb wall. This characterization was used to calculate equivalent porous resistance coefficients for the perforated walls. Separately, 1D theory was used to calculate the same inertial resistance coefficients and corroborated the CFD values within 12.5%. The resistance coefficients from the unit cell CFD model were then used as an input to a second transient CFD model of the whole honeycomb panel as a simplified porous medium. This time-accurate model was run for the whole depressurization event, and predicted a maximum pressure differential between atmosphere and panel of 11.2 kPa. The methodology was designed for speed. It could be applied to a new panel geometry and return time-accurate results of a given depressurization schedule within one working day.

Simcenter Amesim was used to develop a 1D flow network model of the panel. The predicted maximum pressure differential was within 12% of the CFD model result. The CFD methodology was also validated against available data from an experimental test of a sealed honeycomb panel being evacuated from a single location. The results showed agreement within the experimental uncertainty, thereby demonstrating how this workflow correctly captures the complex flow within honeycomb panels undergoing rapid depressurization and provides a powerful, fast new tool in the design of honeycomb panels.

OUTLOOK

The modeling methodology described in this paper has potential to be expanded to more complex scenarios. For instance, including thermals effects using an isothermal inner face sheet and a prescribed temperature decrease on the external face sheet and at region boundaries to better represent launch conditions. In scenarios where hole size or other geometric parameters are uncertain, experimental testing on as-manufactured samples could be used to calibrate the CFD approach and ensure appropriate resistance coefficients are used. Similarly, vent holes in the face sheets, which are commonly used in spacecraft applications, could be represented in the porous CFD model and the efficacy of such holes assessed. More generally, trade studies on the size of honeycomb cell, number and size of perforation, core-ribbon orientation, and number and locations of vent holes could be carried out to optimize composite honeycomb panel design.

REFERENCES

1. Schweickart, R.B., and G. Devaud, "Predicting Spacecraft Component Differential Pressures during Launch," 50th International Conference on Environmental Systems, 12-15 July 2021.
2. Epstein, G and Ruth, S, "Honeycomb Sandwich Structures: Vented versus Unvented Designs for Space Systems", Aerospace Report TR-93(3904), 1993.
3. Mironer, A. and F. Regan, F., "Venting of Space-Shuttle Payloads, Shuttle Environment and Operations Meeting: Collection of Technical Papers", Oct 31-Nov 2, 1983, Washington, D.C., pp. 66-67.
4. Rinker, M., et al., "Analysis of an Aircraft Honeycomb Sandwich Panel with Circular Face Sheet/Core Disbond Subjected to Ground-Air Pressurization."
5. Wu, D., et al., "An Empirical Discharge Coefficient Model for Orifice Flow," International Journal of Fluid Power (2002), Vol. 3, Iss. 3, pp. 13-18.